

Title: Local water year values for the conterminous United States

Running title: CONUS local water years

Authors: Xinyu Sun*¹ and Kendra Spence Cheruvelil^{1,2}

*Corresponding author: Xinyu Sun (16xs6@queensu.ca; sunxiny9@msu.edu)

Affiliation:

1 Department of Fisheries and Wildlife, Michigan State University, 480 Wilson Rd, East Lansing, MI, USA 48824

2 Lyman Briggs College, Michigan State University, 919 E Shaw Ln, East Lansing, Michigan, USA 48825

This paper is a non-peer reviewed preprint submitted to EarthArXiv. The manuscript was submitted to *Limnology & Oceanography Letters* for peer review.

1 **Article type:** Data article

2 **Title:** Local water year values for the conterminous United States

3 **Running title:** CONUS local water years

4 **Authors:** Xinyu Sun*¹ and Kendra Spence Cheruvelil^{1,2}

5 ***Corresponding author:** Xinyu Sun (16xs6@queensu.ca; sunxiny9@msu.edu)

6 **Affiliation:**

7 1 Department of Fisheries and Wildlife, Michigan State University, 480 Wilson Rd, East Lansing,
8 MI, USA 48824

9 2 Lyman Briggs College, Michigan State University, 919 E Shaw Ln, East Lansing, Michigan,
10 USA 48825

11

12 **Author Contribution Statement:** XS and KSC conceived the project and designed the overall
13 approach. XS collected and processed the data, wrote the code, and conducted the spatial
14 interpolation. XS wrote the first draft of the manuscript and both authors reviewed and revised
15 the manuscript.

36 **Abstract:**

37 Quantifying and predicting precipitation and water flow and their influences is challenged by the
38 dynamic relationships between and timing of precipitation and water fluxes. To help with these
39 challenges, scientists use “water year” to examine and predict the impacts of precipitation and
40 relevant extreme climatic and hydrological events on ecosystems. However, traditional water
41 year definitions used in the U.S. lack a consideration of areal variation in climate and hydrology,
42 which is needed when studying ecosystems at regional or national scales. We developed local
43 water year (LWY) values that consider spatial variation using existing definitions whereby the
44 water year begins in the month with the lowest or highest average monthly streamflow. We
45 employed spatial interpolation to assign LWY start and end months to 202 subregions across the
46 conterminous U.S. that range from 4,384 to 134,755 km². This dataset can be linked with diverse
47 climate, terrestrial, and aquatic data for broad-scale studies.

48

49 **Keywords:** Water year; Streamflow; Spatial variation; Spatial interpolation; Macroscale;

50 Precipitation

51

52 **Background & Motivation**

53 Precipitation plays a crucial role in shaping hydrology and ecosystems. Precipitation can
54 be highly spatially variable, especially when considering macroscale spatial extents of regions to
55 continents (Mock 1996; Augustine 2010). As a result of climate change, there has been greater
56 inter-annual variability in precipitation in many regions worldwide (IPCC 2021), causing
57 increased frequency and intensity of extreme climatic and hydrological events such as drought
58 and flooding (Easterling et al. 2000; Grimm & Natori 2006; Prein et al. 2016; Kundzewicz et al.
59 2020). In addition, water fluxes are sometimes asynchronous with precipitation and extreme
60 events can occur during the transition between years, complicating hydrological estimations. For
61 example, rainfall in late fall can be retained in the soil and influence water fluxes the following
62 spring (Pike 1964; Kamps & Heilman 2018). Despite such spatial and temporal variation and
63 asynchronicity in precipitation, a calendar year timeframe (from January 1st to December 31st)
64 has often been used to examine and predict the impacts of precipitation and relevant extreme
65 climatic and hydrological events on aquatic systems.

66 To more accurately predict water flow, researchers adopted a “water year” that usually
67 spans two standard calendar years. For example, the U.S. Geological Service (USGS) water year,
68 which was adopted a century ago, starts on October 1st and ends on September 30th of the next
69 year (Henshaw et al. 1915). This USGS water year is applied to the whole U.S. and intends to
70 account for the influence of snowfall from October to December on the next year’s streamflow
71 (Henshaw et al. 1915). However, different regions of the U.S. have different timing of
72 precipitation (including snowfall) and hydrology, as well as varying topographic patterns, all of
73 which affect relationships between (and timing of) precipitation and water fluxes (Nicótina et al.

74 2008; Condon & Maxwell 2015; Torre Zaffaroni et al. 2023). These facts mean that a more
75 localized timeframe is needed rather than applying a single water year to the macroscale.

76 Researchers have started to use various definitions for water year, and subsequent
77 start/end times of that water year depend on the locations, ecosystem types, and research
78 purposes or questions. For example, Olson et al. (2013) started their water year in April when
79 analyzing the methane and carbon dioxide fluxes of a temperate peatland, Kamps and Heilman
80 (2018) started their water year in September to match annual precipitation with water and carbon
81 budgets in Central Texas, and Caruso (2000) started water years from July or October so that the
82 low-streamflow periods in the Otago region in New Zealand could be fully captured. These (and
83 other) studies use water years for a relatively local spatial extent (e.g., watershed or single region
84). However, organisms and ecological processes are influenced by multi-scale factors, from local
85 (e.g., lake morphometry) to regional (e.g., land use) and macroscale (e.g., climate), and these
86 factors can sometimes interact to affect ecosystems (Heffernan et al. 2014; Rose et al. 2017;
87 LaRue et al. 2021). Thus, it is crucial to investigate and predict how ecosystems respond to
88 environmental changes, such as precipitation variability and relevant extreme events, across
89 multiple spatial and temporal scales. Therefore, localized water year timeframes are needed for a
90 range of research purposes at regional to continental scales.

91 One challenge to creating localized water year timeframes has been limited data for
92 variables such as snow melting time, ice-off dates, and annual gross primary productivity (e.g.,
93 Olson et al. 2013, Kamps & Heilman 2018). However, Wasko et al. (2020) proposed a climate-
94 and hydrology-relevant local water year (LWY) timeframe that solely used streamflow data that
95 are available for most areas globally. This LWY provides a site-specific timeframe beginning in
96 the month with the lowest average monthly streamflow to capture the concurrent and lagged

97 associations between precipitation and hydrology (Wasko et al. 2020). Using this localized
98 timeframe, they predicted the timing and trends of flooding and streamflow at the global scale
99 and demonstrated an improved accuracy of estimation compared with using a calendar year
100 timeframe (Wasko et al. 2020).

101 Although a big step forward for global studies relying on water year data, these data do
102 not completely cover the conterminous U.S. (CONUS), which may limit regional to CONUS-
103 scale research. Thus, we build on their work by extending this local water year timeframe to
104 cover the CONUS. We used recent (1990 to 2018) streamflow data, the same method used by
105 Wasko et al. (2020), and a spatial interpolation method to construct a CONUS-scale LWY
106 timeframe. In addition, given that the most appropriate definition of water year varies depending
107 on research purposes, we applied the same process and generated a second LWY timeframe
108 starting from the month with the highest average monthly streamflow, an approach often used in
109 studies of low streamflow and hydrological drought (e.g., Caruso 2000; Chagas et al. 2024). To
110 create these LWYs, we used subregions that were created based on the drainage features by the
111 USGS (Seaber et al. 2007). This hierarchical regionalization framework divides and subdivides
112 the U.S. into successively smaller hydrologic units (HUs); we used the HU4 subregion, which is
113 the second-level classification that delineates large river basins (USGS 2024). We included 202
114 HU4s in the CONUS that range in area from 4,384 to 134,755 km². These LWY data will help
115 advance the understanding of the impacts of variability in precipitation and streamflow on inland
116 waters at the regional and national U.S. scales.

117

118 **Data Description**

119 This data product consists of two datasets housed on the Environmental Data Initiative
120 (EDI) repository (<https://doi.org/10.6073/pasta/c27e57749f856bd24dc7c7559b9b316b>), as well
121 as our R code (file name: local water year code.R). The first dataset (file name: water years 875
122 sites.csv) was used to develop and evaluate the LWY end month across the CONUS. This file
123 includes the identifier from the Global Runoff Data Centre, which is the archive where we
124 obtained streamflow data (“grdc_no” column), end month of the LWY that begins from the
125 month with the lowest average monthly streamflow (“end.month.lowest” column), end month of
126 the LWY that begins from the month with the highest average monthly streamflow
127 (“end.month.highest” column), and locational information (longitude (“lon” column), latitude
128 (“lat” column), altitude (“altitude” column), and the name of the river (“river” column) and
129 station (“station” column) of each gauging site where the daily streamflow data were measured)
130 (the process of site selection will be described in the next section). There are a total of 875 sites.
131 When the LWY starts from the lowest-flow month, the most common LWY end month among
132 these sites is July (228 sites), followed by August (219 sites), December (160 sites), and
133 September (78 sites) (Figure 1a & 2a). When the LWY starts from the highest-flow month, the
134 most common end month is April (214 sites), followed by February (175 sites), March (145
135 sites), and May (134 sites) (Figure 3a & 4a).

136 The second dataset (file name: hu4 water years with notes.csv) contains the local water
137 year data for each subregion. This file includes the start (“start.month.lowest” column) and end
138 month (“end.month.lowest” column) of the LWY that begins from the month with the lowest
139 average monthly streamflow as well as the start (“start.month.highest” column) and end month
140 (“end.month.highest” column) of the LWY that begins from the month with the highest average
141 monthly streamflow for each of the 202 subregions (i.e., 4-digit Hydrologic Unit; HU4) across

142 the CONUS (“hu4.code” column). This dataset also includes two “notes” columns
143 (“notes.lowest” and “notes.highest”) that provide details about whether there were streamflow
144 data in the subregion and the method we used to determine the LWY end month. There are three
145 categories in this column: 1) dominant_interpolation, which indicates that there were streamflow
146 data and we based the end month on the single, dominant interpolated LWY end month value in
147 the subregion; 2) local_sites_based, which indicates that there were streamflow data and multiple
148 LWY end month values in the subregion; therefore, end month was based on the site-specific
149 LWY data; and 3) ND_interpolation, which indicates that there were no streamflow data in the
150 area and the end month was determined based on the dominant LWY end month value from
151 interpolation of nearest sites. More details about the methodology can be found in sections 3 and
152 4.

153 The results of this work are 404 LWYs, two for each subregion across the CONUS.
154 There are spatial differences in LWY end months (Figure 2b & 4b). For example, along the
155 eastern and western edges of the CONUS, the LWY that begins from the month with the lowest
156 streamflow (hereafter referred to as LWY-lowest) usually ends in July or August, except for the
157 very southeast where it ends in April. In contrast, there is much more heterogeneity in LWY-
158 lowest in the central U.S., with November and December being the most common end months.
159 The most common end month for LWY-lowest is August (64 subregions), followed by July (49
160 subregions), December (34 subregions), and November (16 subregions) among all subregions
161 (Figure 1b). When LWY starts from the highest-flow month (hereafter referred to as LWY-
162 highest), the end months are often February and March in the eastern U.S. and April and May in
163 the central U.S., with more heterogeneity in the western U.S. Among all subregions, the most

164 common LWY-highest end month is February (48 subregions), followed by April (42
165 subregions), March (39 subregions), and May (33 subregions) (Figure 3b).

166

167 **Methods**

168 We first generated subregion-specific LWYs based on the definition and method
169 proposed by Wasko et al. (2020) (i.e., LWY-lowest), in combination with daily streamflow data
170 and spatial interpolation. Then, using the same process, we generated a second LWY timeframe
171 based on a different definition (i.e., LWY-highest). Data processing was performed in R (R Core
172 Team 2024).

173 We used daily streamflow data from the Global Runoff Data Centre (GRDC; GRDC
174 2023) to calculate the monthly streamflow at each site (i.e., river gauge station). The GRDC is an
175 open-access archive of international data that has been widely used in regional, multinational,
176 and global hydrological studies (e.g., Hong et al. 2007; Wasko et al. 2021; Brunner & Slater
177 2022). We first downloaded data from 1990 to 2018 for the CONUS. Then, we filtered the
178 streamflow data for sites that met four criteria to avoid big missing gaps in data, to take into
179 account potential inter-annual variation in streamflow features, and to ensure that the data are
180 relatively ‘recent’: 1) with at least 10 years of data, 2) with at least eight months of data from at
181 least half of the years, 3) average daily streamflow data missing rate was $\leq 80\%$ across all the
182 years, and 4) the last year of data is post-2000. This process resulted in 875 sites spread across
183 the CONUS.

184 *LWY beginning with the lowest streamflow month (LWY-lowest)*

185 For each site, we calculated the average monthly streamflow data and compared these
186 monthly averages to determine the month with the lowest streamflow. This month became the

187 start month of a site’s LWY (i.e., each site has its own lowest-streamflow-month, which is the
188 start month of an LWY; Wasko et al. 2020). Interestingly, although a previous study suggested
189 that low-river-flow timing in some European and U.S. regions exhibit slight inter-annual
190 variation (Floriancic et al. 2021), the end month of the LWY-lowest was consistent from 1990 to
191 2018 across all the sites in our dataset.

192 We then applied ordinary kriging to interpolate site (river gaging station) LWY-lowest
193 end month data (months as integers, 1 through 12) to the whole CONUS using gstat (v2.1-1,
194 Pebesma & Graeler 2023) and raster (v3.6-23, Hijmans et al. 2023) R packages. Ordinary kriging
195 (OK) is a geostatistical technique commonly used to interpolate and map data for unsampled
196 locations and areas (e.g., Sanabria et al. 2013; Boudibi et al. 2019; Li et al. 2023). OK generally
197 involves three steps: computing the semivariogram, defining a semivariogram model, and
198 interpolating based on the semivariogram model (Gimond 2023).

199 We computed the semivariogram, which depicts the spatial correlation between the
200 neighboring values, using equation (1),

$$201 \gamma(h) = \frac{1}{2n} \sum_{i=1}^n [Z(x_i) - Z(x_i + h)]^2 \quad (1)$$

202 where $\gamma(h)$ is the semivariogram; $Z(x_i)$ and $Z(x_i + h)$ are the data at locations x_i and $x_i + h$,
203 respectively; and n is the number of pairs of data separated by distance h (Li & Heap 2011;
204 Sanabria et al. 2013). Second, we fit a mathematical model to the semivariogram. The spherical
205 function was used in our model, and we adjusted parameter values (e.g., partial sill, range, and
206 nugget) to improve the model fit. Third, we applied this semivariogram model to interpolate the
207 LWY-lowest end-month data, by using equations (2) and (3) to estimate the local data (at the
208 unsampled location) using neighboring data,

$$209 Z^*(x_0) = \sum_{i=1}^n \lambda_i Z(x_i) \quad (2)$$

210 $var\{Z^*(x_0) - Z(x_0)\} = \text{minimum} \quad (3)$

211 where $Z^*(x_0)$ is the estimated value at location x_0 ; $Z(x_i)$ is the data value at location x_i ; and λ_i is
212 the weighting factor that is determined by minimizing the variance (equation 3). Finally, we
213 overlaid the interpolated end month LWY-lowest values with subregion polygons for the
214 CONUS to assign the LWY-lowest end month for each subregion.

215 The resulting 202 subregion LWY-lowest values include 156 subregions that were
216 labeled “dominant_interpolation” in the dataset (hu4 water year with notes.csv, “notes.lowest”
217 column). These subregions had streamflow data and a single dominant interpolated LWY-lowest
218 end month in the subregion, so the end month was chosen based on the dominant value. There
219 were 29 subregions labeled as “local_sites_based”, which indicates that there were streamflow
220 data but multiple different LWY-lowest end month values in the subregion. It was difficult to
221 determine the dominant month of these subregions based on interpolation results, thus the
222 decision of the LWY-lowest end month of the subregion was made by checking the site-specific
223 LWY data in each of the subregions and determining the dominant month of each subregion. For
224 the 17 subregions labeled “ND_interpolation”, there was no streamflow data and the month was
225 determined solely based on interpolation results and the dominant interpolated LWY-lowest end
226 month value.

227 *LWY beginning with the highest streamflow month (LWY-highest)*

228 For each site, we used the calculated average monthly streamflow data and compared
229 these monthly averages to determine the month with the highest streamflow, which became the
230 start month of a site’s LWY. When the highest-streamflow-month varied among years for a lake,
231 the start month of a site’s LWY-highest was the highest-streamflow-month with the highest
232 frequency of occurrence. Then, following the processes described above, we applied spatial

233 interpolation and obtained 202 subregion LWY-highest values, including 178 subregions that
234 were labeled “dominant_interpolation” in the dataset (hu4 water year with notes.csv,
235 “notes.highest” column), seven subregions labeled as “local_sites_based”, and 17 subregions
236 labeled “ND_interpolation” (without streamflow data).

237

238 **Technical Validation**

239 We assessed the performance of the spatial interpolation method using a leave-one-out
240 cross-validation approach (Sanabria et al. 2013). Firstly, we randomly chose a site (i.e., river
241 gaging station) and removed its LWY data from the dataset. Then, we applied the ordinary
242 kriging method described above to the new dataset, re-estimated the LWY end month of the
243 removed site, and compared the new estimated LWY end month value with the actual end month.
244 We repeated this process 10 times on 10 different, spatially-separated sites. For both LWY
245 definitions, we found that the estimated and the actual end month of these 10 sites were either the
246 same or differed by one month (mean absolute difference = 0.4 months for LWY-lowest and 0.5
247 months for LWY-highest), depending on the streamflow data density of the subregion.
248 Subregions with a higher data density had higher accuracies than areas with a lower density of
249 data.

250

251 **Data Use and Recommendations for Reuse**

252 This local water year dataset is intended to provide localized, continental-scale water year
253 timeframes that can be used for studying the features and impacts of precipitation and hydrology
254 across the CONUS. It is important to note that precipitation and hydrological dynamics and
255 patterns can vary by the water year definition (e.g., Figure 5). Using the Little Fork River in

256 Minnesota (USA) as an example, if a researcher was studying the peak streamflow in April 2001,
257 it would be in water year 2002 when using either LWY-lowest or LWY-highest, but in water
258 year 2001 when using the water year created by USGS (Oct 1st - Sep 30th). Thus, it is crucial to
259 choose a water year definition that matches the context and research question being asked. The
260 LWY-lowest can be useful for studying the relationship between precipitation and runoff and
261 local long-term hydrological cycles (e.g., water replenishment and depletion cycle). The LWY-
262 highest can provide more relevant insights for research focused on dry or low-flow periods
263 because it covers the entire low-streamflow period. Finally, in some cases, an alternative
264 definition could be more useful. For example, the USGS water year definition that starts from
265 October 1st might be appropriate for hydrological studies in snow-dominated regions.

266 Here, we provide an example of using these three different timeframes to identify the
267 water years with the lowest and highest annual average streamflow from water years 1991-2018.
268 We assigned each of the 875 sites two LWY end months (LWY-lowest and LWY-highest)
269 according to the subregion they are located in (i.e., all the sites in the same subregion share the
270 same end month; Sun & Cheruvilil 2024), calculated the annual average streamflows of each site
271 based on these two LWY timeframes, and then determined the water years with the highest and
272 lowest streamflow for each site and timeframe. Then, we calculated the site-specific annual
273 average streamflow based on the water year that ends on September 30th (USGS) and
274 determined the water years with the highest and lowest streamflow for each site using that
275 definition of water year. Finally, we compared the highest and lowest streamflow water years
276 between LWY-lowest and the Oct-Sep water year (by USGS) and between LWY-highest and the
277 Oct-Sep water year (by USGS). For all the three definitions, the water year was named by the
278 calendar year in which it ended (e.g., the 12-month period from August 1st, 2010 to July 31st,

279 2011 = LWY 2011). We found that, for some sites across the CONUS, the water years with the
280 lowest and highest annual average streamflow were consistent across water year definitions,
281 while for others, these years varied (Figure 6). Additionally, the comparison between LWY-
282 highest and USGS Oct-Sep water year definition resulted in more sites with different highest and
283 lowest streamflow years (Figure 6 b&d; 75% and 68% were different for the highest and lowest
284 streamflow years, respectively) than the comparison between LWY-lowest and Oct-Sep water
285 year created by USGS (Figure 6 a&c; 25% and 24% for the highest and lowest streamflow years,
286 respectively). These results suggest that the water year definition can influence the identification
287 of extreme streamflow events and highlight the importance of selecting appropriate definitions.

288 This LWY dataset considers areal variations and can be used in various meteorological,
289 hydrological, and ecological studies to identify and predict trends in precipitation, extreme
290 events (drought and flooding), and water fluxes as well as investigate their effects on ecosystems
291 (e.g., Kamps & Heilman 2018) and human communities (e.g., calculating hydropower generation
292 capacity; Bongio et al. 2016). Future users of the subregion-specific LWYs can combine these
293 data with a wide range of climatic, as well as terrestrial and aquatic abiotic and biotic data, by
294 linking our dataset with other data products, such as LAGOS-US modules (e.g., Cheruvilil et al.
295 2021) or USGS datasets (e.g., Blodgett 2023) using subregion identifiers (i.e., HU4 codes).
296 Moreover, our R code is available for download at the EDI repository so that users can apply a
297 similar method to other regions around the world to generate site or region-specific LWY
298 timeframes. As such, these data will be a valuable addition to the literature that can contribute to
299 building macroscale understanding of precipitation and streamflow variability and their
300 influences on a variety of systems.

301

302

303 **Conflict of interest:** The authors declare no conflict of interest.

304

305 **Acknowledgments:** We thank Dr. Conrad Wasko and his colleagues for kindly guiding us on
306 how to download data from GRDC and sharing data with us. This work was supported by the
307 U.S. National Science Foundation (NSF) Macrosystems Biology & NEON-Enabled Science
308 Program (DEB #1638679).

309 **References**

- 310 Augustine, D. J. (2010). Spatial versus temporal variation in precipitation in a semiarid
311 ecosystem. *Landscape Ecology*, 25(6), 913–925. <https://doi.org/10.1007/s10980-010-9469-y>
- 312 Blodgett, D. L. (2023). *Twelve-digit hydrologic unit soil moisture, recharge, actual*
313 *evapotranspiration, and snowpack water equivalent storage from the National Hydrologic*
314 *Model Infrastructure with the Precipitation-Runoff Modeling System 1980-2016.*
315 <https://doi.org/10.5066/P9W148A1>
- 316 Bongio, M., Avanzi, F., & De Michele, C. (2016). Hydroelectric power generation in an Alpine
317 basin: Future water-energy scenarios in a run-of-the-river plant. *Advances in Water*
318 *Resources*, 94, 318–331. <https://doi.org/10.1016/j.advwatres.2016.05.017>
- 319 Boudibi, S., Sakaa, B., & Zapata-Sierra, A. J. (2019). Groundwater quality assessment using GIS,
320 ordinary kriging and WQI in an arid area. *PONTE International Scientific Researchs Journal*,
321 75(12). <https://doi.org/10.21506/j.ponte.2019.12.14>
- 322 Brunner, M. I., & Slater, L. J. (2022). Extreme floods in Europe: Going beyond observations
323 using reforecast ensemble pooling. *Hydrology and Earth System Sciences*, 26(2), 469–482.
324 <https://doi.org/10.5194/hess-26-469-2022>
- 325 Caruso, B. S. (2000). Evaluation of low-flow frequency analysis methods. *Journal of Hydrology*
326 (New Zealand), 39(1), 19–47. <https://www.jstor.org/stable/43944831>
- 327 Chagas, V. B. P., Chaffe, P. L. B., & Blöschl, G. (2024). Regional Low Flow Hydrology: Model
328 Development and Evaluation. *Water Resources Research*, 60(2), e2023WR035063.
329 <https://doi.org/10.1029/2023WR035063>
- 330 Cheruvilil, K. S., Soranno, P. A., McCullough, I. M., Webster, K. E., Rodriguez, L. K., & Smith,
331 N. J. (2021). LAGOS-US LOCUS v1.0: Data module of location, identifiers, and physical

332 characteristics of lakes and their watersheds in the conterminous U.S. *Limnology and*
333 *Oceanography Letters*, 6(5), 270–292. <https://doi.org/10.1002/lol2.10203>

334 Condon, L. E., & Maxwell, R. M. (2015). Evaluating the relationship between topography and
335 groundwater using outputs from a continental-scale integrated hydrology model. *Water*
336 *Resources Research*, 51(8), 6602–6621. <https://doi.org/10.1002/2014WR016774>

337 Easterling, D. R., Meehl, G. A., Parmesan, C., Changnon, S. A., Karl, T. R., & Mearns, L. O.
338 (2000). Climate extremes: Observations, modeling, and impacts. *Science*, 289(5487), 2068–
339 2074. <https://doi.org/10.1126/science.289.5487.2068>

340 Floriancic, M. G., Berghuijs, W. R., Molnar, P., & Kirchner, J. W. (2021). Seasonality and
341 drivers of low flows across Europe and the United States. *Water Resources Research*, 57(9),
342 e2019WR026928. <https://doi.org/10.1029/2019WR026928>

343 Gimond, M. (2023). *Intro to GIS and spatial analysis*.
344 <https://mgimond.github.io/Spatial/index.html>.

345 GRDC. (2023). *GRDC - The Global Runoff Data Centre*.
346 https://grdc.bafg.de/GRDC/EN/Home/homepage_node.html

347 Grimm, A. M., & Natori, A. A. (2006). Climate change and interannual variability of
348 precipitation in South America. *Geophysical Research Letters*, 33(19), 2006GL026821.
349 <https://doi.org/10.1029/2006GL026821>

350 Heffernan, J. B., Soranno, P. A., Angilletta, M. J., Buckley, L. B., Gruner, D. S., Keitt, T. H.,
351 Kellner, J. R., Kominoski, J. S., Rocha, A. V., Xiao, J., Harms, T. K., Goring, S. J., Koenig,
352 L. E., McDowell, W. H., Powell, H., Richardson, A. D., Stow, C. A., Vargas, R., & Weathers,
353 K. C. (2014). Macrosystems ecology: Understanding ecological patterns and processes at

354 continental scales. *Frontiers in Ecology and the Environment*, 12(1), 5–14.
355 <https://doi.org/10.1890/130017>

356 Hendrickson, W. A., & Ward, K. B. (1975). Atomic models for the polypeptide backbones of
357 myohemerythrin and hemerythrin. *Biochemical and Biophysical Research Communications*,
358 66(4), 1349–1356. [https://doi.org/10.1016/0006-291x\(75\)90508-2](https://doi.org/10.1016/0006-291x(75)90508-2)

359 Henshaw, F. F., Baldwin, G. C., Stevens, G. C., & Fuller, E. S. (1915). *Surface water supply of*
360 *the United States, 1911* (Water Supply Paper). U.S. Geological Service.
361 <https://doi.org/10.3133/wsp312>

362 Hijmans, R. J., Etten, J. van, Sumner, M., Cheng, J., Baston, D., Bevan, A., Bivand, R., Busetto,
363 L., Canty, M., Fasoli, B., Forrest, D., Ghosh, A., Golicher, D., Gray, J., Greenberg, J. A.,
364 Hiemstra, P., Hingee, K., Ilich, A., Geosciences, I. for M. A., ... Wueest, R. (2023). *raster*:
365 *Geographic Data Analysis and Modeling* (3.6-23). [https://cran.r-](https://cran.r-project.org/web/packages/raster/index.html)
366 [project.org/web/packages/raster/index.html](https://cran.r-project.org/web/packages/raster/index.html)

367 Hong, Y., Adler, R. F., Hossain, F., Curtis, S., & Huffman, G. J. (2007). A first approach to
368 global runoff simulation using satellite rainfall estimation. *Water Resources Research*, 43(8),
369 2006WR005739. <https://doi.org/10.1029/2006WR005739>

370 Intergovernmental Panel On Climate Change. (2021). *Climate Change 2021 – The Physical*
371 *Science Basis: Working Group I Contribution to the Sixth Assessment Report of the*
372 *Intergovernmental Panel on Climate Change*. Cambridge University Press.
373 <https://doi.org/10.1017/9781009157896>

374 Kamps, R. H., & Heilman, J. L. (2018). A method to calculate a locally relevant water year for
375 ecohydrological studies using eddy covariance data. *Ecohydrology*, 11(7), e1980.
376 <https://doi.org/10.1002/eco.1980>

377 Kidder, G. W., & Montgomery, C. W. (1975). Oxygenation of frog gastric mucosa in vitro. *The*
378 *American Journal of Physiology*, 229(6), 1510–1513.
379 <https://doi.org/10.1152/ajplegacy.1975.229.6.1510>

380 Kundzewicz, Z. W., Huang, J., Pinskiwar, I., Su, B., Szwed, M., & Jiang, T. (2020). Climate
381 variability and floods in China - A review. *Earth-Science Reviews*, 211, 103434.
382 <https://doi.org/10.1016/j.earscirev.2020.103434>

383 LaRue, E. A., Rohr, J., Knott, J., Dodds, W. K., Dahlin, K. M., Thorp, J. H., Johnson, J. S.,
384 Rodríguez González, M. I., Hardiman, B. S., Keller, M., Fahey, R. T., Atkins, J. W.,
385 Tromboni, F., SanClements, M. D., Parker, G., Liu, J., & Fei, S. (2021). The evolution of
386 macrosystems biology. *Frontiers in Ecology and the Environment*, 19(1), 11–19.
387 <https://doi.org/10.1002/fee.2288>

388 Li, J., & Heap, A. D. (2011). A review of comparative studies of spatial interpolation methods in
389 environmental sciences: Performance and impact factors. *Ecological Informatics*, 6(3–4),
390 228–241. <https://doi.org/10.1016/j.ecoinf.2010.12.003>

391 Li, L., Sun, J., Wang, H., Ouyang, Y., Zhang, J., Li, T., Wei, Y., Gong, W., Zhou, X., & Zhang,
392 B. (2023). Spatial distribution and temporal trends of dietary niacin intake in Chinese
393 residents ≥ 5 years of age between 1991 and 2018. *Nutrients*, 15(3), 638.
394 <https://doi.org/10.3390/nu15030638>

395 Mock, C. J. (1996). Climatic controls and spatial variations of precipitation in the western United
396 States. *Journal of Climate*, 9(5), 1111–1125. [https://doi.org/10.1175/1520-](https://doi.org/10.1175/1520-0442(1996)009<1111:CCASVO>2.0.CO;2)
397 [0442\(1996\)009<1111:CCASVO>2.0.CO;2](https://doi.org/10.1175/1520-0442(1996)009<1111:CCASVO>2.0.CO;2)

398 Nicóтина, L., Alessi Celegon, E., Rinaldo, A., & Marani, M. (2008). On the impact of rainfall
399 patterns on the hydrologic response. *Water Resources Research*, 44(12), 2007WR006654.
400 <https://doi.org/10.1029/2007WR006654>

401 Olson, D. M., Griffis, T. J., Noormets, A., Kolka, R., & Chen, J. (2013). Interannual, seasonal,
402 and retrospective analysis of the methane and carbon dioxide budgets of a temperate peatland.
403 *Journal of Geophysical Research: Biogeosciences*, 118(1), 226–238.
404 <https://doi.org/10.1002/jgrg.20031>

405 Pebesma, E., & Graeler, B. (2023). *gstat: Spatial and Spatio-Temporal Geostatistical Modelling,*
406 *Prediction and Simulation (2.1-1)*. <https://github.com/r-spatial/gstat/>

407 Pike, J. G. (1964). The estimation of annual run-off from meteorological data in a tropical
408 climate. *Journal of Hydrology*, 2(2), 116–123. [https://doi.org/10.1016/0022-1694\(64\)90022-](https://doi.org/10.1016/0022-1694(64)90022-8)
409 8

410 Prein, A. F., Holland, G. J., Rasmussen, R. M., Clark, M. P., & Tye, M. R. (2016). Running dry:
411 The U.S. Southwest’s drift into a drier climate state. *Geophysical Research Letters*, 43(3),
412 1272–1279. <https://doi.org/10.1002/2015GL066727>

413 R Core Team. (2024). *R: A language and environment for statistical computing*. R Foundation
414 for Statistical Computing. <https://www.r-project.org/>

415 Rajcáni, J., Krobová, J., & Málková, D. (1975). Distribution of Lednice (Yaba 1) virus in the
416 chick embryo. *Acta Virologica*, 19(6), 467–472.

417 Rose, K. C., Graves, R. A., Hansen, W. D., Harvey, B. J., Qiu, J., Wood, S. A., Ziter, C., &
418 Turner, M. G. (2017). Historical foundations and future directions in macrosystems ecology.
419 *Ecology Letters*, 20(2), 147–157. <https://doi.org/10.1111/ele.12717>

420 Sanabria, L. A., Qin, X., Li, J., Cechet, R. P., & Lucas, C. (2013). Spatial interpolation of
421 McArthur's forest fire danger index across Australia: Observational study. *Environmental*
422 *Modelling & Software*, 50, 37–50. <https://doi.org/10.1016/j.envsoft.2013.08.012>

423 Seaber, P. R., Kapinos, F. P., & Knapp, G. L. (2007). *Hydrologic Unit Maps*. U.S. Geological
424 Survey. <https://pubs.usgs.gov/wsp/wsp2294/>
425

426 Sun, X., & Cheruvilil, K. S. (2024). *Local water years for 4-digit hydrologic unit areas across*
427 *the conterminous United States*. Environmental Data Initiative.
428 <https://portal.edirepository.org/nis/mapbrowse?packageid=edi.1547.3>. Last accessed in
429 February 2025

430 Torre Zaffaroni, P., Baldi, G., Texeira, M., Di Bella, C. M., & Jobbágy, E. G. (2023). The timing
431 of global floods and its association with climate and topography. *Water Resources Research*,
432 59(7), e2022WR032968. <https://doi.org/10.1029/2022WR032968>

433 USGS. (2024). *Water resources of the United States: Hydrologic unit maps*.
434 <https://Water.USgs.Gov/GIS/Huc.Html>. <https://water.usgs.gov/GIS/huc.html>

435 Wasko, C., Nathan, R., & Peel, M. C. (2020). Trends in global flood and streamflow timing
436 based on local water year. *Water Resources Research*, 56(8), e2020WR027233.
437 <https://doi.org/10.1029/2020WR027233>

438 Wasko, C., Nathan, R., Stein, L., & O'Shea, D. (2021). Evidence of shorter more extreme
439 rainfalls and increased flood variability under climate change. *Journal of Hydrology*, 603,
440 126994. <https://doi.org/10.1016/j.jhydrol.2021.126994>

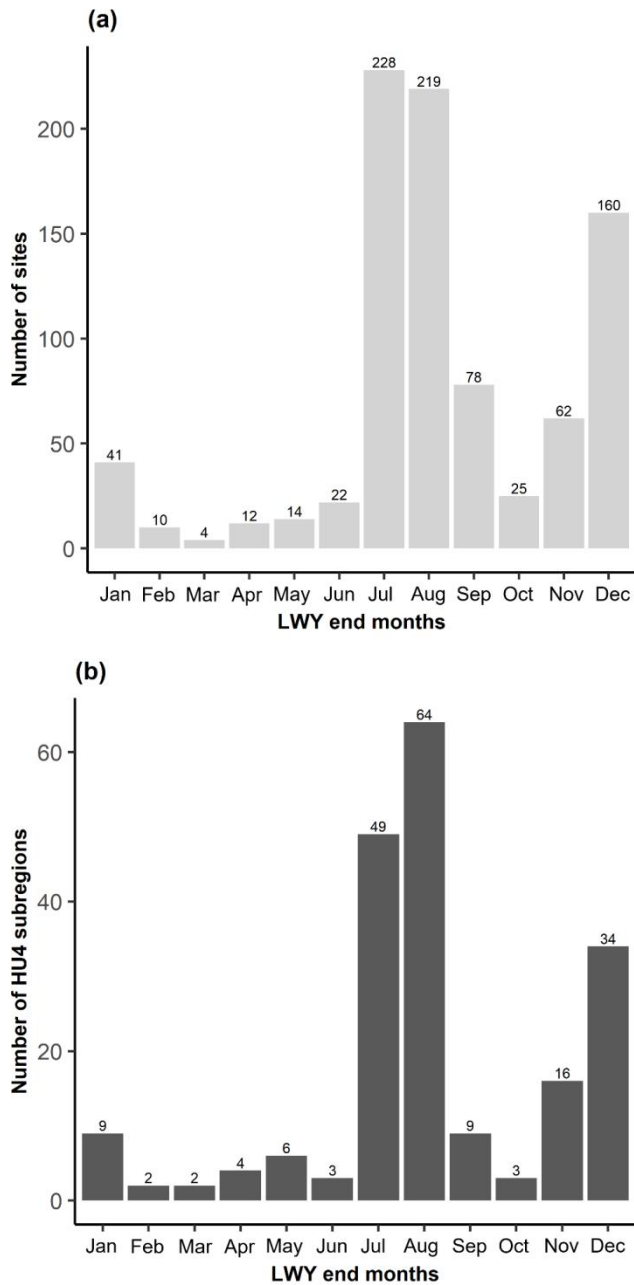
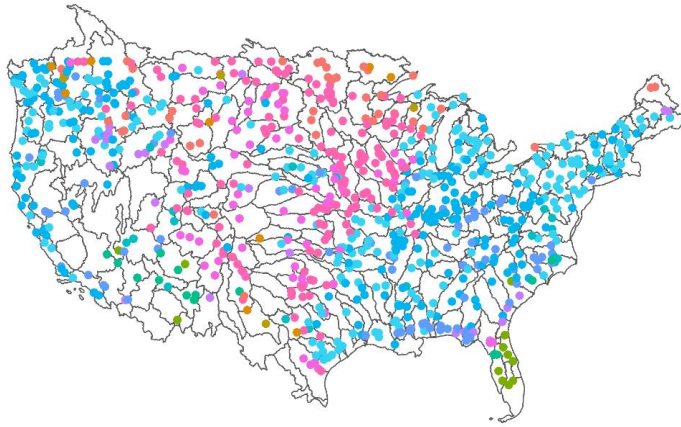
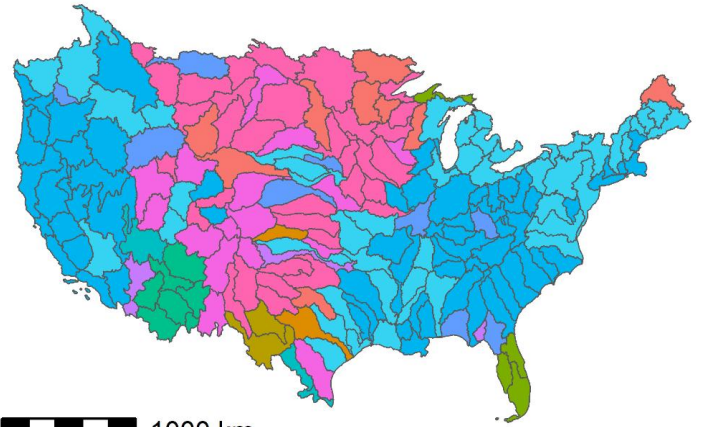


Figure 1. The number of stream gauging sites (a) and subregions (b) by the end month of the local water year (LWY) that starts from the month with the lowest average monthly streamflow (LWY-lowest). The numbers above each bar indicate the number of sites (top) or subregions (bottom). Subregion = HU4 (Seaber et al. 2007). More information about HU4s can be found on the USGS website: <https://water.usgs.gov/GIS/huc.html>, last accessed September 2023.

(a)



(b)



1000 km

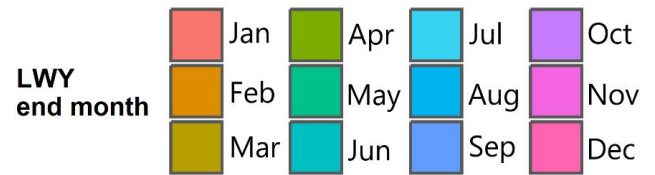


Figure 2. Maps showing the LWY-lowest end month of each site overlaid with subregion (HU4) polygons (a) and the end month for each subregion (b). The LWY starts from the month with the lowest average monthly streamflow. In plot (a), there are 17 subregions without streamflow data. Colors represent the end months.

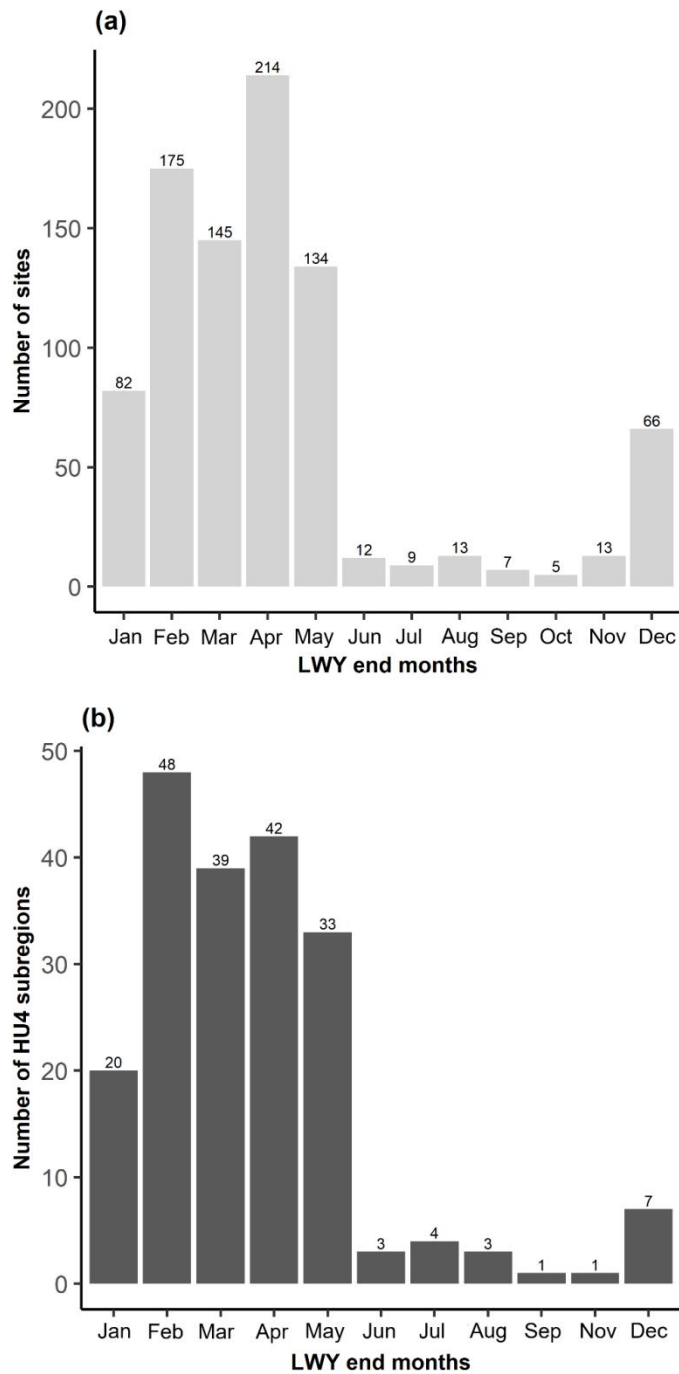


Figure 3. The number of stream gauging sites (a) and subregions (b) by the end month of the local water year (LWY) that starts from the month with the highest average monthly streamflow (LWY-highest). The numbers above each bar indicate the number of sites (top) or subregions (HU4; bottom).

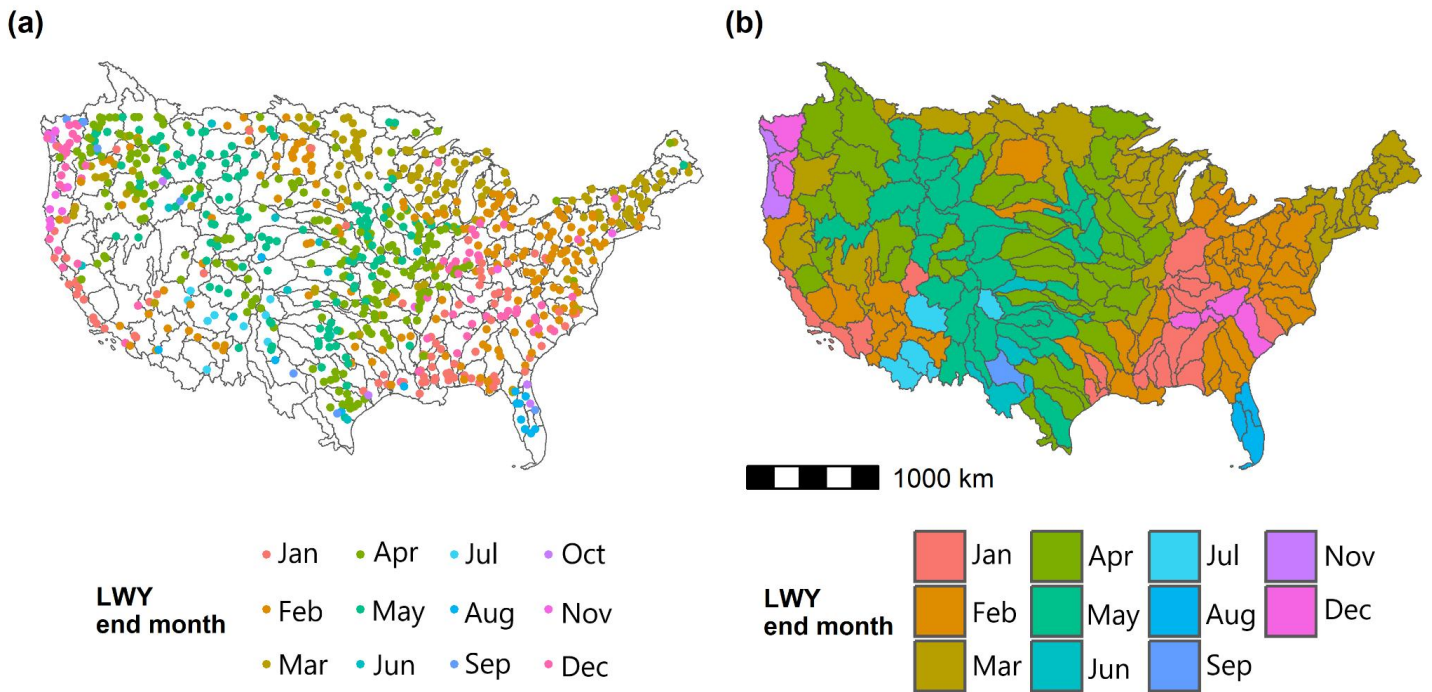


Figure 4. Maps showing the LWY-highest end month of each site overlaid with subregion (HU4) polygons (a) and the end month for each subregion (b). The LWY starts from the month with the lowest average monthly streamflow. Colors represent the end months.

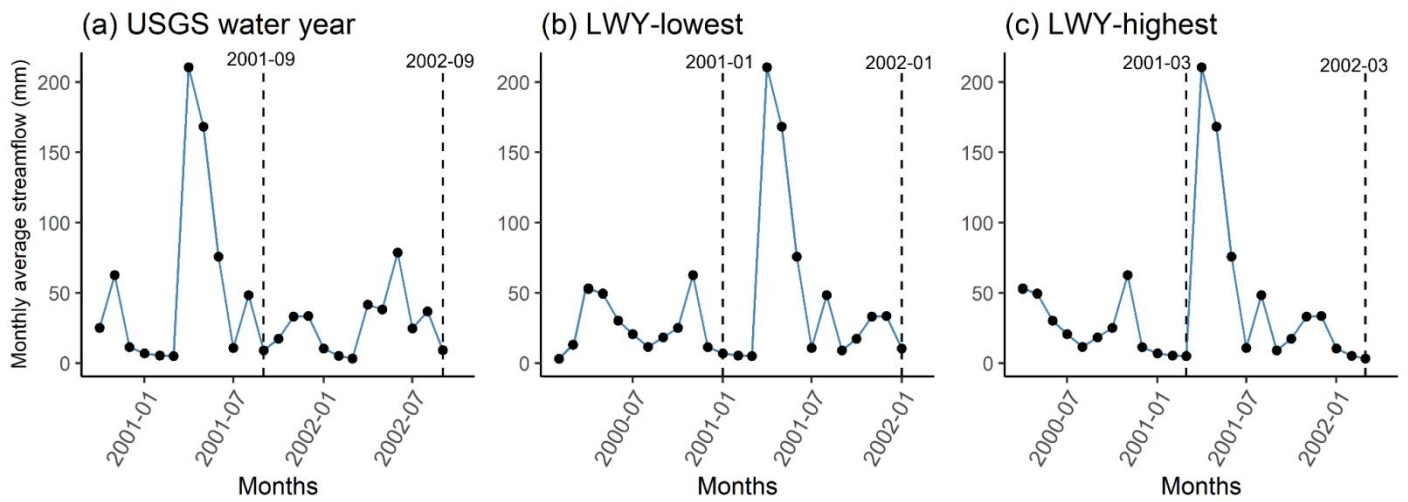


Figure 5. Monthly average streamflow data of Little Fork River (Minnesota, USA, latitude=48.3958, longitude=-93.5493) in the water years 2001 and 2002 using three LWY definitions: Oct 1st - Sep 30th water year (sensu USGS) (a), LWY-lowest (b), and LWY-highest (c). The dashed lines indicate the end month of the water years.

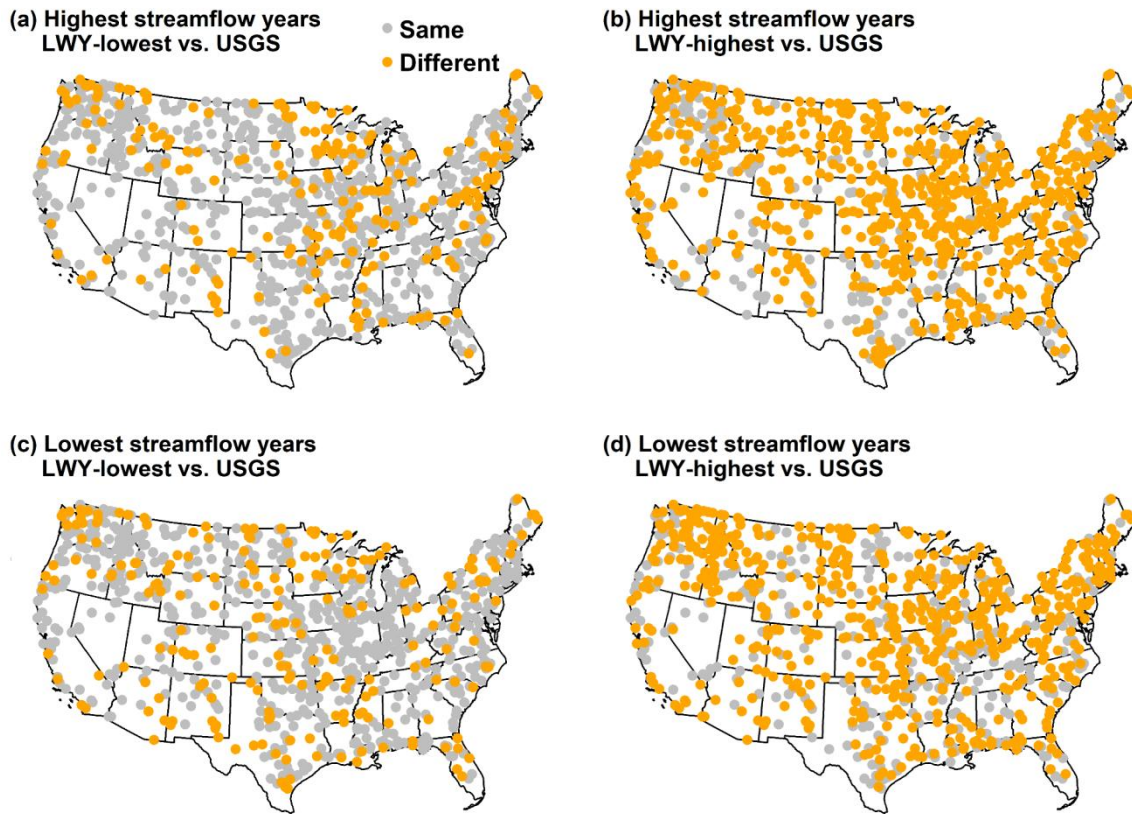


Figure 6. Maps showing the comparison of the highest/lowest streamflow water years across the three water year definitions. Plots (a) and (b) show whether the year with the highest streamflow was the same or different for each site when using different water year definitions. Plot (a) compares LWY-lowest with the Oct - Sep (USGS) water year definition, while plot (b) compares LWY-highest with the Oct - Sep water year. Plots (c) and (d) show whether the year with the lowest streamflow was the same or different for each site when using different water year definitions. Plot (c) compares LWY-lowest with the Oct - Sep water year definition, while plot (d) compares LWY-highest with the Oct - Sep water year. Grey dots indicate that the years were the same between the definitions, and orange dots indicate that the years were different.